# Characterization of a hyperspectral imager

Jonathan M. Mooney and William S. Ewing
Air Force Research Laboratory
Hanscom AFB, MA 01731

## ABSTRACT

A spectral imager constructs a three dimensional (two spatial and one spectral) image from a series of two dimensional images. This paper discusses a technique for spectral imaging that multiplexes the spatial and spectral information on a staring focal plane, then demultiplexes the resulting imagery to obtain the spectral image. This approach has high optical throughput and is robust to focal plane array (FPA) nonuniformities. This presentation is the third in a series to the IRIS passive sensors community. Previously we introduced the hardware and discussed the reconstruction algorithm in detail. Here we review the hardware and present experimental results.

## 1. INTRODUCTION

Often objects of similar intensity have different spectral signatures which can be used to distinguish between them. This work is motivated by our desire to perform spectral discrimination in the mid-wave infrared. From previous experience we know that infrared scenes consist of low contrast details on a large background pedestal, and that focal plane array (FPA) nonuniformities and low optical throughput often limit the performance of infrared spectral imagers [1]. Our goal is to address these potential performance limiting issues by incorporating both a throughput and a multiplex advantage into a spectral imager, and at the same time address the effect of FPA nonuniformity on spectral imaging.

Typical state-of-the-art spectral imagers image the spectrum of a slit onto a 2-dimensional focal plane array; the slit is scanned over the object to create a 3-dimensional spectral image [2]. Since only a slit is imaged at a time, the out-of-slit photons are rejected, hence these spectral imagers are inherently inefficient. Further, pixel-to-pixel nonuniformities on the FPA can corrupt the spectral imagery and reduce the ultimate performance.

The spectral imager we study is similar to previously reported chromotomographic devices [3, 4, 5, 6, 7], all of which image a dispersed view of the entire scene over all of the spectral bands, then computationally reconstruct the chromatic image. In chromotomography the color imagery is considered to be pseudo-three dimensional. The 3D spectral image is obtained using tomographic imaging techniques similar to those used in medical imaging. While chromotomography is computationally demanding, it has the advantage that a slit field stop is not required. We anticipate the spectral imager performance will reflect the larger optical throughput afforded by a larger field stop. The actual performance and potential multiplex advantage (or disadvantage), depend on how well the reconstruction algorithms perform.

Our technique differs from other chromotomographic approaches in several ways: we utilize a direct vision prism to disperse the light; we have derived a reconstruction method that is uniquely suited to

# REPORT DOCUMENTATION PAGE

Form Approved OMB No. 0704-0188



| 1. REPORT DATE (DD-MM-YYYY) | 2. REPORT TYPE | 3. DATES COVERED (FROM - TO) |
|---|---|---|
| 01-01-1998 | Conference Proceedings | xx-xx-1998 to xx-xx-1998 |

4. TITLE AND SUBTITLE
Characterization of a hyperspectral imager
Unclassified

5a. CONTRACT NUMBER
5b. GRANT NUMBER
5c. PROGRAM ELEMENT NUMBER

6. AUTHOR(S)
Mooney, Jonathan M. ;
Ewing, William S. ;

5d. PROJECT NUMBER
5e. TASK NUMBER
5f. WORK UNIT NUMBER

7. PERFORMING ORGANIZATION NAME AND ADDRESS
Air Force Research Laboratory
Hanscom AFB, MA01731

8. PERFORMING ORGANIZATION REPORT NUMBER

9. SPONSORING/MONITORING AGENCY NAME AND ADDRESS
Director, CECOM RDEC
Night Vision and electronic Sensors Directorate, Security Team
10221 Burbeck Road
Ft. Belvoir, VA22060-5806

10. SPONSOR/MONITOR'S ACRONYM(S)
11. SPONSOR/MONITOR'S REPORT NUMBER(S)

12. DISTRIBUTION/AVAILABILITY STATEMENT
APUBLIC RELEASE
,

13. SUPPLEMENTARY NOTES
See Also ADM201041, 1998 IRIS Proceedings on CD-ROM.

14. ABSTRACT
A general method is described for achieving super resolution imagery from multiple frame image sequences that contain motion. The method assumes low-noise, focal plane array imagery recorded with uncontrolled image motion that can included some random jitter. Using this approach, moderate resolution, fast frame image sequences can be processed to achieve high-resolution image sequences displayed at conventional frame rates. The super resolution processing depends only on the imagery, requiring no externally controlled micro-dither or a priori information such as the sensor motion or range to the background. Typical sensor stabilization requirements are relaxed using this method, however, to achieve optimum performance there are some constraints on the motion. Specifically, the stabilization must still good enough so that the resulting random dither is only a few pixels and must be statistically well behaved. Processing examples are given using previously recorded image sequences from a wide FOV MWIR staring array sensor on-board an aircraft.

15. SUBJECT TERMS

| 16. SECURITY CLASSIFICATION OF: | | | 17. LIMITATION OF ABSTRACT | 18. NUMBER OF PAGES | 19. NAME OF RESPONSIBLE PERSON |
|---|---|---|---|---|---|
| a. REPORT | b. ABSTRACT | c. THIS PAGE | Public Release | 9 | Fenster, Lynn<br>lfenster@dtic.mil |
| Unclassified | Unclassified | Unclassified | | | 19b. TELEPHONE NUMBER<br>International Area Code<br>Area Code Telephone Number<br>703767-9007<br>DSN<br>427-9007 |

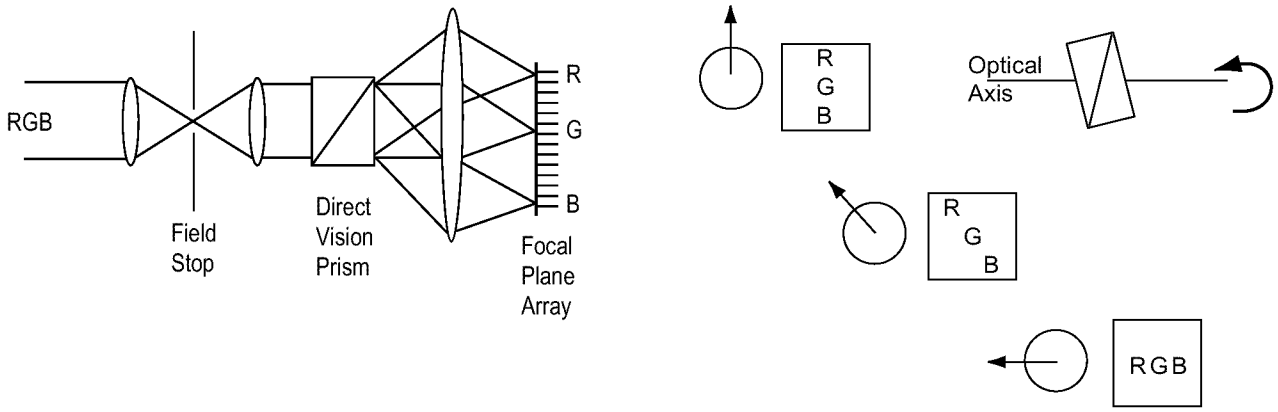


Figure 1: A schematic representation of the spectral imager and its operation. On the left the direct vision prism is shown spreading red, green and blue light across the FPA. On the right the effect of the prism rotation on the overlapping red, green and blue images is illustrated. The circle and arrow represent the prism orientation.

our hardware configuration [8]; we have developed some new ideas for dealing with some of the limitations of chromotomography, and have applied principal component analysis to the characterization of our experimental data. Here we describe the hardware, the reconstruction technique, and the limitations of our approach. We demonstrate infrared spectral imaging and demonstrate infrared spectral discrimination. We will also demonstrate that the imager is robust to the FPA nonuniformities that often limit infrared imager performance.

## 2. HARDWARE CONFIGURATION AND RECONSTRUCTION TECHNIQUE

Figure 1 is a schematic representation of our approach. It consists of a telescope, a direct vision prism and a camera. A direct vision prism consists of two prisms that are arranged such that one wavelength passes through undeviated while other wavelengths are deviated along a line. The direct vision prism is mounted in a bearing so that it can be rotated around the optical axis. As the prism rotates the spectral features in the image will trace out circles where the radius of the circles are wavelength dependent. To obtain a spectral image, a series of frames of camera data are obtained with the prism in different angular orientations, then a computer is used to extract the spectral image from the measured data.

If in Fig. 1 the field stop were replaced by a slit, the prism mount were fixed, and a mechanism for linearly scanning the scene added, then the modified system would be a standard scanned-slit spectral imager. In both cases the throughput is determined by the $f/\#$ and the field stop area. Since the $f/\#$'s are the same and the field stop area is much larger for the angularly multiplexed configuration, it has higher throughput.

In its current configuration the spectral imager gathers one frame of data from each of 80 prism orientations uniformly spaced over $2\pi$. The $f/4$ InSb camera operates at 60 fps with a 2ms integration time. Complete sequences of data are gathered in 1.33s with a composite integration of 160ms. Future configurations could increase the frame rate to improve the dwell efficiency of the instrument. Frame rates of up to 500 fps could be achieved without significant degradation of the imager performance. At

these high frame rates, complete spectral images could be obtained at near real-time rates (complete spectral images in less than 0.2s).

The algorithm used to reconstruct the spectral imagery from the raw data is combination of a direct inverse and an iterative algorithm[9]. The advantage of the combined approach is that the known characteristics of spectral imagery can be utilized to overcome some of the potential limitations of the tomographic approach. Currently the reconstruction algorithm is implemented on a two processor Pentium Pro computer. Complete reconstructions are currently obtained in less than three minutes; however a significant reduction in the run-time could be achieved by sacrificing flexibility.

## 3. EXAMPLE IMAGERY

In order to evaluate the capabilities of the instrument, we imaged a target of opportunity (a building) from a laboratory window. The data was obtained on January 12, 1998 at 9:30 in the morning. In order to minimize the effects of FPA nonuniformities and stray reflections from the rotating prism, an additional sequence of data was recorded with the entrance pupil blocked. The blocked sequence was used to perform a one-point nonuniformity correction on a frame-by-frame basis. This type of nonuniformity correction reduces the ultimate signal to noise ratio by a factor of $\sqrt{2}$. Development of an optimal nonuniformity correction technique remains for future work.

Examples of the dispersed imagery is shown in Fig. 2. The angular orientation of the prism is reflected in the imagery by a anisotropic blurring in the direction of prism dispersion. Sharp edges in the scene are sharply imaged only when the prism orientation matches that of the edge. Since edges are sharply focused for some of the prism orientations, the information about the edges is not lost in the same sense that it is lost when the imagery is defocused. (This differentiates tomography from image enhancement.)

Also evident in the raw data is the effect of atmospheric absorption by $CO_2$. The effect is clearly visible in the 90 deg orientation image as a horizontal dark band separating two bright regions.

Figure 3 illustrates 6 of the 64 spectral reconstructions. Though there are 64 samples, only 33 of them are statistically independent (due to filtering in the reconstruction algorithm[8]); therefore the spectral resolution is approximately 0.06 $\mu m$ or 40 $cm^{-1}$. Spectral profiles of a selection of pixels in

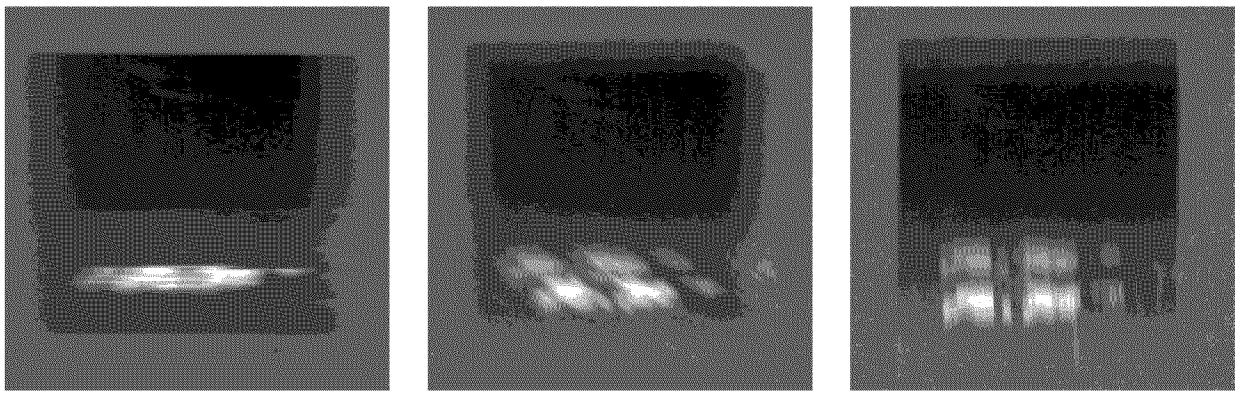

Figure 2: Three images of the Eighty frame sequence. The prism orientations were 0, 45 and 90 deg.

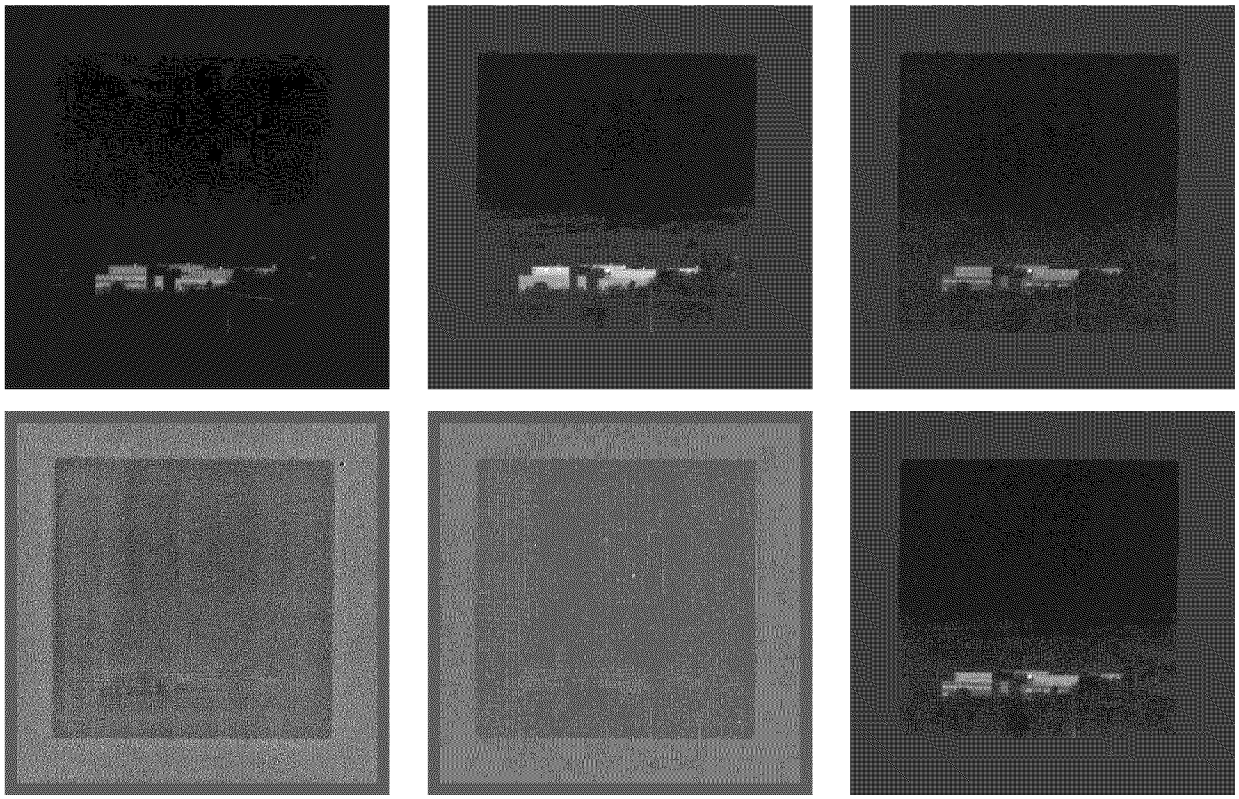

Figure 3: Spectral reconstructions. From right to left across the top row 3.52, 3.95, and 4.14$\mu m$, and 4.25, 4.38 and 4.62$\mu m$ across the bottom row.

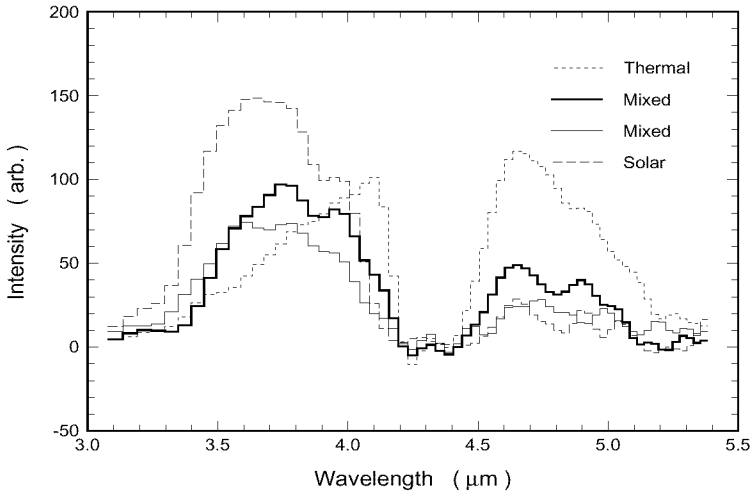


Figure 4: Spectral profiles of four pixels in the image. The profile labeled 'Solar' is that of an aluminum vent on the roof. The profile labeled 'thermal' is that of an air conditioning unit also on the roof. The two mixed profiles are from different sections of wall, one brick and the other painted metal.

the image are illustrated in Fig. 4. The spectral profiles are taken from sequences of data after the mean of each frame has been subtracted on a frame-by-frame basis. The mean removal highlights the spectral features at the expense of the monotonic upward trend in intensity from the 3 to 5 $\mu m$.

Solar radiation dominates the 3.0 $\mu m$ side of the band, and thermal emission dominates the 5.0 $\mu m$ side. In general the cross-over depends on the time of day, the weather and the ambient temperature. For our scene the cross-over occurs at 3.95 $\mu m$; the effect of which can be seen in the reversal of contrast of the windows on the building in the sequence of images. The vents on the roof are visible at 3.52 $\mu m$ but not at 4.62 $\mu m$, while the converse is true for the air conditioner.

The strong effect of atmospheric absorption over the 4.2-4.5 $\mu m$ band is observed as a dramatic reduction in contrast in the imagery, and as zero intensity on the spectral profiles (where the spatial mean has been removed). The spectral profiles also exhibit the broadening of the absorption band with range. The thermal signatures are emitted at the building, and must pass through only the atmosphere between the building and the camera. The solar profiles, being reflected, must pass through the atmosphere between the sun and the building, then pass through the atmosphere between the building and the camera. The observed profiles exhibit the effects of the different path lengths. (Another example for very short paths is illustrated in Fig. 7.)

An artifact of the instrument that is nearly coincident with the $CO_2$ absorption band is the effect of the FPA nonuniformities. The direct vision prism has been constructed such that the light at 4.38 $\mu m$ passes through undeviated. Consequently, as the prism rotates, the portion of the spectral image near 4.38 $\mu m$ remains fixed on the focal plane. As far as the inversion algorithm is concerned, there is no way to distinguish between the focal-plane-array nonuniformities and the 4.38 $\mu m$ light. Therefore the effect of the nonuniformities is mapped into the 4.38 $\mu m$ spectral band. If the undeviated wavelength is designed to coincide with a strong absorption band, then the effect of the focal plane nonuniformities on the spectral discrimination function can be minimized.

The spectral profiles shown in Fig. 4 provide a way of verifying the spectral resolution. The spectral feature present as a shoulder in the thermal profile and as a dip in one of the mixed profiles at 4.9 $\mu m$ is due to the atmosphere. MODTRAN atmospheric absorption simulations indicate that if the spectral resolution were much poorer than 20 $cm^{-1}$ the feature would not be visible. Our Calculations indicate that at 4.9 $\mu m$ the spectral resolution should be 24 $cm^{-1}$. We conclude that the spectral resolution is close to the design resolution.

By design the spectral resolution near 3 $\mu m$ is 110 $cm^{-1}$. The variation in spectral resolution as a function of wavelength is due to the nonlinear dispersion of the direct vision prism. On average, the spectral resolution across the 3-5 $\mu m$ band is 40 $cm^{-1}$.

## 4. PRINCIPAL COMPONENT ANALYSIS AND END-MEMBERS

A widely used tool for finding correlations and locating anomalies in a data set is Principal Component Analysis (PCA)[10]. The goal of PCA as applied to spectral imaging is to uncover band-to-band correlations among the spectral images, then identify a set of spectra and corresponding images that have no mutual correlation, but can still fully represent the spectral imagery. PCA is an effective tool in hyperspectral image processing because spectral images exhibit a large degree of correlation. Once the strongly correlated features are grouped together, the anomalous features become more

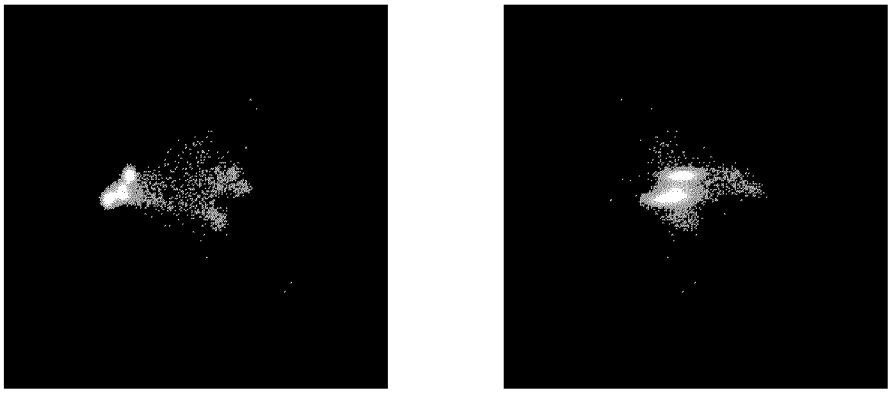

Figure 5: Two views of the hyperspectral image scatter plot. The left image illustrates the first eigenimage intensity versus the second. The right image illustrates the second versus fourth. The third eigenimage represents focal plane array nonuniformities.

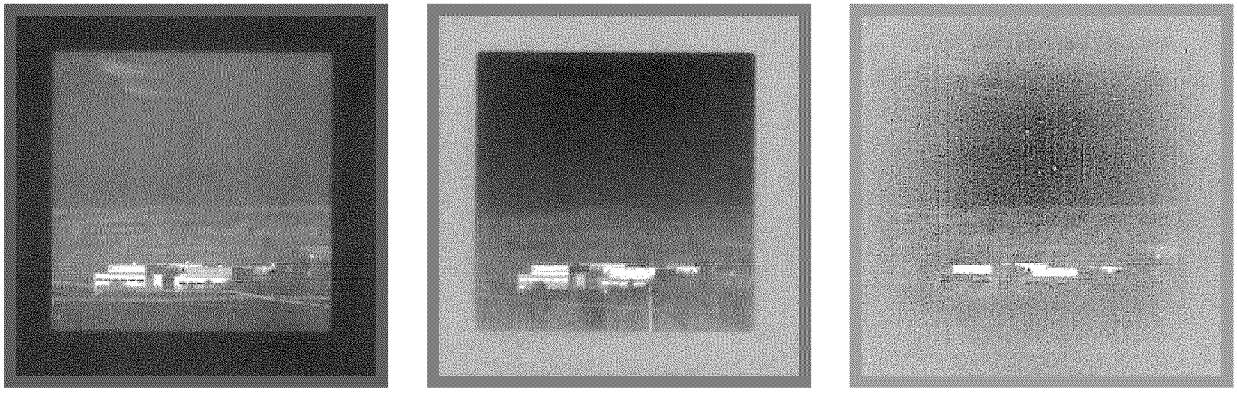

Figure 6: Images of three of the end-members of the hyperspectral imagery. From left to right the images correspond to the 'Solar', 'Thermal', and 'Painted Metal' end-members.

pronounced.

The process of PCA involves identifying an orthonormal basis of eigenspectra. Each of the eigenspectra has a corresponding eigenimage. The intensity of a pixel in a given eigenimage establishes the intensity of the corresponding eigenspectrum for that pixel. Figure 5 is a scatter plot where each pixel is represented by a bright point, and the coordinates of the point are established by two eigenimage intensities. Pixels with similar spectral signatures form clusters on the scatter plot.

The three bright clusters in the left image of Fig. 5 are due to the field stop, the ground and the sky. One can imagine the three bright clusters as one vertex of a larger triangle that envelops all of the points in the scatter plot. The top vertex of the triangle represents those pixels that have a solar dominated spectrum, the bottom vertex represents those pixels that have a thermal dominated spectrum, and the left vertex, with the three large clusters, represents the reference from which the other points are measured. The vertices of this triangle represent the end-members of our hyperspectral image. They are the purest examples of spectral behavior that is anomalous from the background pixels. Spectral profiles of the two pixels closest to the vertices of the triangle are labeled 'Solar' and 'Thermal' in

Fig. 4. The right image in Fig. 5 exposes an additional end-member, that due is to the painted metal structure on the roof of the building. Images of these three end-members are shown in Fig. 6.

## 5. PERFORMANCE CHARACTERIZATION

Consider the schematic representation of our instrument in Fig. 1. If the square field stop were replaced by a slit with the thin dimension aligned in the direction of prism dispersion, the hardware would be configured as a scanned slit instrument. Since the optics, camera and electronics are identical, a comparison of the performance in the two configurations will provide a measure of the tomographic spectral imager performance relative to that of a scanned slit instrument.

Such a comparison is made in Fig. 7. A uniform target was measured in both configurations. The data in the scanned slit configuration was obtained from one row of pixels. The calibration is identical in each case and was obtained by averaging over 50 rows and over 64 frames of the scanned slit data. A comparison of the two plots in Fig. 7 indicates that the performance of the tomographic approach is superior to that of the scanned slit by nearly a factor of 3.

If the slit in this experiment were cold, then the performance of the scanned slit configuration may improve relative to the tomographic configuration. A cold slit would have eliminated the thermal emission from the slit, which would lead to a reduction in the noise due to the background flux. In general, we conclude that the performance of the tomographic approach will be superior to that of a scanned slit when the noise is not dominated by the shot noise of the signal photo-electrons. In addition to a warm slit, short data acquisition time, low flux levels and limited optical aperture can keep an optical system from being signal shot noise limited. If the performance were signal shot noise limited, the performance of tomographic technique would be approximately a factor of 3 poorer than that of the scanned slit for the current reconstruction algorithm. We are hopeful that future improvements will lead to an even more favorable comparison.

Figure 8 illustrates the Modulation Transfer Function of both the infrared camera and the spectrometer as measured using the modified knife-edge technique [11]. (The infrared camera was measured with the re-imaging relay, and without the prism.) The comparison shows that MTF is unaffected by the tomographic reconstruction for spatial frequencies below 1/2 Nyquist. However, above 1/2 Nyquist some degree of degradation is present.

## 6. CONCLUSIONS

The tomographic approach to spectral imaging provides high-fidelity data with simple hardware. There is no need for a slit in the tomographic approach which significantly enhances the optical throughput and removes any potential requirement for cooling the slit or any of the optics.

The average spectral resolution across the 3-5 $\mu m$ band is approximately 40 $cm^{-1}$. Near 5 $\mu m$ the spectral resolution is comparable to the 20 $cm^{-1}$ design limit of the LOTRAN atmospheric model.

The spatial resolution of the reconstructed spectral imagery is only marginally degraded relative to the pan-chromatic imagery taken with the same hardware. The signal to noise ratio of the resulting

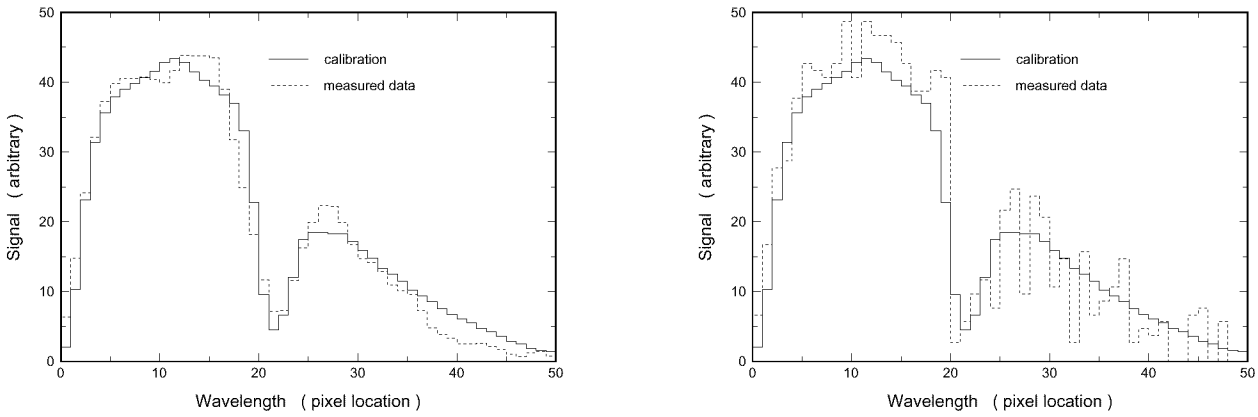


Figure 7: Comparison of spectral profiles obtained with the tomographic configuration (left) and in a scanned slit configuration (right).

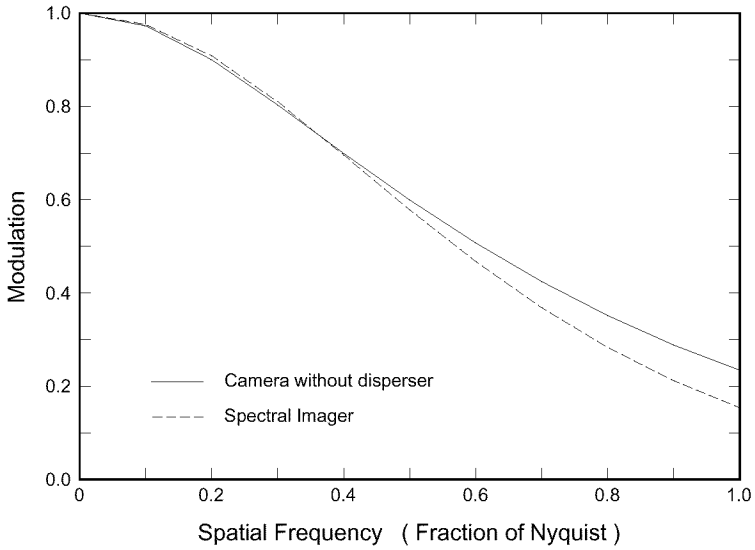


Figure 8: Measured MTF of the infrared camera and the spectral imager.

imagery is superior to that of read-noise limited scanned slit configurations that utilize the same hardware.

## 7. ACKNOWLEDGMENTS

The authors thank Andrzej Brodzik for help in developing the reconstruction algorithm; Steven DiSalvo for help in fabricating the infrared camera; Virgil Vickers for software support; and Jerry Silverman, Paul Pellegrini and Freeman Shepherd for critical reading of this manuscript. This work was supported by AFOSR Task 2305CR under Dr. Gerry Witt.

## 8. REFERENCES

[1] J. Mooney, F. Shepherd, W. Ewing, J. Murguia, and J. Silverman, "Responsivity nonuniformity limited performance of infrared staring cameras," *Optical Engineering*, vol. 28, pp. 1151–1161, November (1989).

[2] R. Basedow, D. Carmer, and M. Anderson, "Hydice systems, implementation and performance," in *Imaging Spectrometry I* (M. R. Descour, J. M. Mooney, D. L. Perry, and L. Illing, eds.), vol. 2480, pp. 258–267, (1995).

[3] G. G. Levin and G. N. Vishnyakov, "On the possibilities of chronotomography of high speed processes," *Optics Communications*, vol. 56, pp. 231–234, December (1985).

[4] T. Okamoto, A. Takahashi, and I. Yamaguchi, "Simultaneous acquisition of spectral and spatial intensity distribution," *Applied Spectroscopy*, vol. 47, pp. 1198–1202, August (1993).

[5] Y. Betremieux, T. A. Cook, D. M. Cotton, and S. Chakrabarti, "Spinr: two-dimensional spectral imaging through tomographic reconstruction," *Optical Engineering*, vol. 32, pp. 3133–3138, December (1993).

[6] M. Descour and E. Dereniak, "Computed-tomography imaging spectrometer: experimental calibration and reconstruction results," *Applied Optics*, vol. 34, pp. 4817–4826, August (1995).

[7] P. A. Bernhardt, "Direct reconstruction methods for hyperspectral imaging with rotational spectrotomography," *J. Opt. Soc. Am. A*, vol. 12, pp. 1884–1901, September (1995).

[8] J. M. Mooney, V. E. Vickers, M. An, and A. K. Brodzik, "High-throughput hyperspectral infrared camera," *Journal of the Optical Society of America*, vol. 14, pp. 2951–2961, November (1997).

[9] J. M. Mooney, A. K. Brodzik, and M. An, "Principal component analysis in limited angle chromotomography," in *Imaging Spectrometry III* (M. R. Descour and S. S. Shen, eds.), vol. 3118, pp. 170–178, (1997).

[10] I. T. Jolliffe, *Principal Component Analysis*. New York: Springer-Verlag, (1986).

[11] A. P. Tzannes and J. M. Mooney, "Measurement of the modulation transfer function of infrared cameras," *Optical Eng.*, vol. 34, pp. 1808–1817, June (1995).